Coronal Shock Waves, EUV waves, and their Relation to CMEs. II. Modeling MHD Shock Wave Propagation Along the Solar Surface by Using Nonlinear Geometrical Acoustics

An.N. Afanasyev · A.M. Uralov

Abstract We model propagation of a coronal shock wave by using nonlinear geometrical acoustics. The method is based on the WKB approach and takes into account main properties of nonlinear waves: *i*) dependence of the wave front velocity on the wave amplitude, *ii*) nonlinear dissipation of the wave energy, and *iii*) progressive increase in the duration of solitary shock waves. We address the method in detail and present results of modeling propagation of shock-associated EUV waves as well as Moreton waves along the solar surface in the simplest solar corona model. The calculations reveal deceleration and lengthening of the waves. In contrast, waves considered in the linear approximation keep their length unchanged and slightly accelerate.

Keywords: Magnetohydrodynamics; Waves, Propagation; Waves, Shock

1. Introduction

Many solar eruptive events appear to initiate MHD waves in the corona. This conjecture is supported by observations of a few kinds of their manifestations. First, these are waves visible in chromospheric spectral lines. For several decades, there have been known Moreton waves (Moreton and Ramsey, 1960) observed in the Hα line. Uchida (1968) proposed that a Moreton wave represented a chromospheric trail of a coronal fast-mode wave. More recent studies show a probable coronal nature of Moreton waves (*e.g.*, Balasubramaniam, Pevtsov, and Neidig, 2007). Similar phenomena are propagating waves observed in the He I 10830 Å line (*e.g.*, Vršnak *et al.*, 2002b; Gilbert *et al.*, 2004). Second, type II radio bursts are considered to be signatures of coronal shock waves propagating upwards in the corona (Uchida, 1960). Furthermore, presumable signatures of coronal waves can be observed in soft X-rays (Narukage *et al.*, 2002; Khan and Aurass, 2002; Hudson *et al.*, 2003; Warmuth, Mann, and Aurass,

Institute of Solar-Terrestrial Physics SB RAS,
P.O. Box 291, Lermontov St. 126A, Irkutsk 664033, Russia
email: afa@iszf.irk.ru email: uralov@iszf.irk.ru

2005), microwaves (Warmuth *et al.*, 2004a; White and Thompson, 2005), and metric radio-wavelengths (Vršnak *et al.*, 2005).

Other candidates to be visualizations of coronal MHD waves are large-scale wave-like disturbances discovered in 1998 with the Extreme-ultraviolet Imaging Telescope (EIT) and referred to as "EIT waves" or "EUV waves". This term appears to include phenomena having the different physical nature and therefore various morphological and dynamical properties. For more details, we refer the reader to Introduction in companion Paper I (Grechnev *et al.*, 2010b). Note here only that describing EUV waves in terms of fast-mode MHD waves seems to be possible and correct for those cases when we really deal with "wave" phenomena. Just this class of EUV transients is a subject of our consideration.

Thus, fast-mode MHD waves are responsible for a number of solar transients and it is important to describe their propagation through the corona. But there remain some questions about modeling the waves.

In his original approach, Uchida (1968) modeled a coronal disturbance as a linear and short fast-mode MHD wave propagating from a point source. To calculate a dome-like surface of the wave front and find the position of a Moreton wave (as an intersection line of the dome and the solar surface), he used the linear geometric acoustics [the WKB (Wentzel–Kramers–Brillouin) approach]. Some recent studies (*e.g.*, Wang, 2000; Patsourakos *et al.*, 2009) also used the same approach under the assumption of a linear disturbance. In this consideration, a disturbance moves along rays, which curve into regions of a reduced Alfvén speed. This results in the appearance of wave "imprints" (*e.g.*, Moreton waves) running along the spherical solar surface. Note that in the linear approximation an amplitude and duration of the wave do not affect the shape of the wave front and the speed of its motion along the rays. Neither amplitude nor duration of the wave were calculated in the mentioned papers; the geometry of propagation only was of interest.

The Uchida's model of a linear MHD wave has demonstrated a possibility to describe Moreton waves in these terms. Later papers of Uchida with collaborators (Uchida, Altschuler, and Newkirk, 1973; Uchida, 1974) and recent papers (Wang, 2000; Patsourakos *et al.*, 2009), in which the coronal magnetic field was calculated from photospheric magnetograms, provided more accurate quantitative description of Moreton and EUV waves in terms of the linear model.

However, the linear model predicts acceleration of Moreton and EUV waves, whereas observations show their systematic deceleration (Warmuth *et al.* 2001; 2004a). Also, it is often pointed out by many authors that the speeds of Moreton waves sometimes well exceed the fast-mode ones (Narukage *et al.*, 2002; Narukage *et al.*, 2004; Warmuth *et al.*, 2004b; Muhr *et al.*, 2010). Furthermore, velocities of coronal waves, which are estimated from observed drifts of type II radio bursts, indicate an obvious excess above the expected fast-mode speed in the corona (*e.g.*, Warmuth *et al.*, 2004b; Vršnak *et al.*, 2002a and references therein). These facts suggest that the linear approximation does not always correctly describe propagation of those waves. Probably, a disturbance responsible for the transients listed above is nonlinear and most likely is a shock wave.

Studies of propagation of shock waves meets difficulties due to their nonlinearity. Analytic methods to describe propagation of shock waves are approximate

and often describe the behavior of some extreme classes of nonlinear waves (*e.g.*, very strong self-similar waves, or weak waves, *etc.*).

Grechnev *et al.* (2008; 2010b) discuss a possibility to formally describe decelerating EUV waves as strong self-similar waves in a medium with a power-law density falloff from a wave source. This assumption seems to be exotic because the velocity of such a wave should significantly exceed the fast-mode speed. However, unlike the case of a solitary weak shock, permanent mass increase of gas involved in a motion away from the source is inherent for a self-similar wave. In impulsive events, such a motion of gas precedes the stage of a weak solitary blast wave. For example, in the point-like explosion theory, this motion corresponds to the stage of a strong self-similar shock wave, with the mass of involved gas being equal to that of gas inside the sphere bounded by the expanding shock front. In solving the initial-value problem of excitation of a linear wave by a sphere of increased pressure, such a gas motion corresponds to the formation stage of the gas compression phase. This compression phase is a leading part of a spherical solitary N-shaped blast wave. In the case of an impulsively expanding spherical piston, formation of a blast wave can occur in a similar manner. This consideration shows possible increase in the plasma mass trailing a shock front at the initial propagation stage of a coronal wave. Probably for this reason, the self-similar approximation provides satisfactory results when used to fit deceleration of Moreton and EUV waves as well as drift rates of metric type II bursts.

At large distances from its source, the disturbance inevitably decays and its speed becomes close to the fast-mode one. This asymptotics is typical for non-self-similar shock waves having a moderate or weak intensity as well as waves, in which a discontinuity has not yet been formed.

The present Paper is devoted to the case of a weak shock wave that appears to be the most acceptable (*e.g.*, Warmuth *et al.*, 2004b; Vršnak *et al.*, 2002a). We do not discuss the appearance of a shock wave. Vršnak and Lulić (2000) approximately described this process, based on an analogy with an accelerating flat piston. The cases of cylindrical and spherical pistons were analyzed by Žic *et al.* (2008). Temmer *et al.* (2009) demonstrated how one could describe the kinematics of a Moreton wave by using the solution of a simple wave without a discontinuity. In our study, we assume that a fast-mode shock wave of a moderate intensity appears during a solar eruption on the periphery of an active region and decays to a weak shock when traveling in the corona. The wave manifests as a Moreton wave and an EUV wave on the solar disk. We calculate propagation of the shock wave in terms of the WKB approach taking account of nonlinear effects.

Such a method in its generally accepted variant involves two independent procedures. In the first one, ray trajectories corresponding to the linear approximation as well as cross-sections of ray tubes are calculated. So, the influence of the finite wave amplitude on the wave front shape and ray trajectories is ignored because in the linear acoustics the propagation velocities of disturbances are equal to the undisturbed sound speed regardless of their amplitude. In the second procedure, a nonlinear variation of the wave amplitude and duration are computed along the linear rays obtained. Such a non-self-consistent approach is fairly useful in some cases, however, nonlinearity effects altering the ray pattern and

the wave velocity disappear completely. Therefore, we develop another method that allows us to consider self-consistently wave propagation and a nonlinear variation of wave characteristics.

The method is considered in Section 2. In Section 3 we formulate the task and present results of analytic modeling propagation of Moreton and EUV waves along the solar surface. Section 4 contains concluding remarks about the method and the results. Note that those who are not interested in mathematical details of the method can read Section 3 without going in details presented in Section 2.

2. Method

The method of nonlinear geometrical acoustics is based on the method of linear geometrical acoustics and allows one to calculate propagation of disturbances with small (but finite) amplitudes through an inhomogeneous medium. The linear geometrical acoustics is known to be a method to calculate linear disturbances in the ray approximation (*e.g.*, Landau and Lifshitz, 1987). In this approximation, a solution is found in a form of $A\left(\mathbf{r},t\right)e^{i\Psi(\mathbf{r},t)}$ where $A\left(\mathbf{r},t\right)$ is the wave amplitude, and $\Psi\left(\mathbf{r},t\right)$ is the eikonal, both depending on coordinates and time. By substituting this representation for wave perturbations into the system of linearized equations of ideal magnetohydrodynamics, one can obtain a Hamilton-Jacobi partial differential equation for the eikonal of fast and slow magnetosonic waves:

$$\frac{\partial\Psi}{\partial t} + (\mathbf{V}\mathrm{grad}\Psi) + a\left|\mathrm{grad}\Psi\right| = 0,$$

where $\mathbf{V}$ is the undisturbed plasma flow velocity (*e.g.*, the solar wind velocity), and a is the magnetosonic speed in plasma. Solving the equation with the method of characteristics gives a system of ray equations, which in spherical coordinates (r,θ,φ) takes the form (Uralova and Uralov, 1994):

$$\begin{aligned}
\frac{dr}{dt} &= V_r + a\frac{k_r}{k} + k\frac{\partial a}{\partial k_r}, \\
r\frac{d\theta}{dt} &= a\frac{k_\theta}{k} + k\frac{\partial a}{\partial k_\theta}, \\
r\sin\theta\frac{d\varphi}{dt} &= a\frac{k_\varphi}{k} + k\frac{\partial a}{\partial k_\varphi}, \\
\frac{dk_r}{dt} &= -\frac{\partial V_r}{\partial r}k_r - \frac{\partial a}{\partial r}k + \frac{a}{kr}\left(k_\theta^2 + k_\varphi^2\right), \\
r\frac{dk_\theta}{dt} &= -\frac{\partial V_r}{\partial\theta}k_r - \frac{\partial a}{\partial\theta}k + \frac{a}{k}k_\varphi^2\cot\theta - k_\theta\frac{dr}{dt}, \\
r\sin\theta\frac{dk_\varphi}{dt} &= -\frac{\partial V_r}{\partial\varphi}k_r - \frac{\partial a}{\partial\varphi}k - \sin\theta k_\varphi\frac{dr}{dt} - k_\varphi r\cos\theta\frac{d\theta}{dt},
\end{aligned} \tag{1}$$

where $k_{r,\theta,\varphi}$ are the components of the wave vector $\mathbf{k} = \mathrm{grad}\Psi$, and k is its magnitude. The equation system (1) corresponds to the case of a medium in

steady-state, where only the radial component V_r of the undisturbed plasma flow exists. By integrating the system (1), one can determine the wave front shape.

This approach has been used for modeling coronal fast-mode MHD waves (Uchida, 1968; Wang, 2000), with only a ray pattern being calculated. However, it is essential not only to find the wave geometry, but also to calculate the wave intensity. The geometrical acoustics allows the wave amplitude variation to be calculated.

In the linear geometrical acoustics, the energy flux of a disturbance traveling in an immovable medium with a group velocity of $\mathbf{q}_0$ is directed along the rays, and its magnitude is conserved within a ray tube (Blokhintsev, 1981), $\mathrm{div}(\Delta\varepsilon\mathbf{q}_0) = 0$, where $\Delta\varepsilon$ is the average density of the disturbance energy. In a medium moving at a velocity of $\mathbf{V}$, we have to take into account the fact that the wave front phase velocity varies as $q_n = V_n + a$, with the n index denoting the projection normal to the front. The conservation law in this case is $\mathrm{div}(\Delta\varepsilon\mathbf{q}\,q_n/a) = 0$ (Uralov, 1982; Barnes, 1992) where $\mathbf{q} = \mathbf{V} + \mathbf{q}_0$ is the group velocity in a moving medium. The average density of the disturbance energy is $\Delta\varepsilon = \rho\overline{(u^2 + v^2)}$ where ρ is the undisturbed plasma density, and u, v are the plasma velocity components along the normal to the wave front and across it, respectively. Taking account of the relation between plasma velocity components $\mu = v/u$ (Kulikovsky and Lyubimov, 2005), it is possible to relate a variation of the wave amplitude to the normal cross-section dS of the ray tube formed by a bundle of close rays:

$$dSq\rho u^2 \left(1 + \mu^2\right) \frac{q_n}{a} = const. \tag{2}$$

Thus, the general approach to determine the wave amplitude in the ray method relies on calculating the ray tube cross-section.

There are various techniques for calculating cross-sections. They are discussed in Kravtsov and Orlov (1990). We calculate cross-sections by using the Jacobian of the transformation to ray coordinates. The volume element dW of a ray tube is expressed in terms of ray coordinates (η_1, η_2, t) as:

$$dW = dxdydz = r^2 \sin\theta drd\theta d\varphi = r^2 \sin\theta D\left(t\right) d\eta_1 d\eta_2 dt,$$

where $D(t)$ is the Jacobian of the transformation from spherical coordinates to ray ones. Then for the ray tube cross-section dS we have:

$$dS = \frac{dW}{d\sigma} = r^2 \sin\theta \frac{D\left(t\right)}{q} d\eta_1 d\eta_2,$$

where σ is the ray tube length. Substituting it into (2) yields:

$$D\left(t\right) r^2 \sin\theta \rho u^2 \left(1 + \mu^2\right) \frac{q_n}{a} = const. \tag{3}$$

To calculate the Jacobian, we use a method based on numerical integrating the so-called adjoint to (1) equation system. This system consists of differential equations for the derivatives $\partial r/\partial\eta_{1,2}$, $\partial\theta/\partial\eta_{1,2}$, $\partial\varphi/\partial\eta_{1,2}$, $\partial k_r/\partial\eta_{1,2}$, $\partial k_\theta/\partial\eta_{1,2}$,

$\partial k_\varphi / \partial \eta_{1,2}$ and is derived from (1) by differentiating the equations with respect to ray coordinates η_1 and η_2. For the case considered, the adjoint system has the following form (in view of the symmetry about η_1 and η_2, instead of twelve equations we give only six for one variable η):

$$\frac{d}{dt}\left(\frac{\partial r}{\partial \eta}\right) = \frac{\partial V_r}{\partial \eta} + \frac{k_r}{k}\frac{\partial a}{\partial \eta} + \frac{a}{k}\frac{\partial k_r}{\partial \eta} - \frac{ak_r}{k^2}\frac{\partial k}{\partial \eta} + \frac{\partial a}{\partial k_r}\frac{\partial k}{d\eta} + k\frac{\partial}{\partial \eta}\left(\frac{\partial a}{\partial k_r}\right),$$

$$\frac{\partial r}{\partial \eta}\frac{d\theta}{dt} + r\frac{d}{dt}\left(\frac{\partial \theta}{\partial \eta}\right) = \frac{k_\theta}{k}\frac{\partial a}{\partial \eta} + \frac{a}{k}\frac{\partial k_\theta}{\partial \eta} - \frac{ak_\theta}{k^2}\frac{\partial k}{\partial \eta} + \frac{\partial a}{\partial k_\theta}\frac{\partial k}{\partial \eta} + k\frac{\partial}{\partial \eta}\left(\frac{\partial a}{\partial k_\theta}\right),$$

$$\frac{\partial r}{\partial \eta}\sin\theta\frac{d\varphi}{dt} + r\cos\theta\frac{\partial \theta}{\partial \eta}\frac{d\varphi}{dt} + r\sin\theta\frac{d}{dt}\left(\frac{\partial \varphi}{\partial \eta}\right) =$$

$$= \frac{\partial a}{\partial \eta}\frac{k_\varphi}{k} + \frac{a}{k}\frac{\partial k_\varphi}{\partial \eta} - \frac{ak_\varphi}{k^2}\frac{\partial k}{\partial \eta} + \frac{\partial a}{\partial k_\varphi}\frac{\partial k}{\partial \eta} + k\frac{\partial}{\partial \eta}\left(\frac{\partial a}{\partial k_\varphi}\right),$$

$$\frac{d}{dt}\left(\frac{\partial k_r}{\partial \eta}\right) = -\frac{\partial V_r}{\partial r}\frac{\partial k_r}{\partial \eta} - k_r\frac{\partial}{\partial \eta}\left(\frac{\partial V_r}{\partial r}\right) - \frac{\partial a}{\partial r}\frac{\partial k}{\partial \eta} - k\frac{\partial}{\partial \eta}\left(\frac{\partial a}{\partial r}\right) + \frac{\partial a}{\partial \eta}\frac{k_\theta^2 + k_\varphi^2}{kr} -$$

$$-\frac{a}{k^2 r}\left(k_\theta^2 + k_\varphi^2\right)\frac{\partial k}{\partial \eta} - \frac{a\left(k_\theta^2 + k_\varphi^2\right)}{kr^2}\frac{\partial r}{\partial \eta} + \frac{a}{kr}\left(2k_\theta\frac{\partial k_\theta}{\partial \eta} + 2k_\varphi\frac{\partial k_\theta}{\partial \eta}\right),$$

$$\frac{\partial r}{\partial \eta}\frac{dk_\theta}{dt} + r\frac{d}{dt}\left(\frac{\partial k_\theta}{\partial \eta}\right) = -\frac{\partial V_r}{\partial \theta}\frac{\partial k_r}{\partial \eta} - k_r\frac{\partial}{\partial \eta}\left(\frac{\partial V_r}{\partial \theta}\right) - \frac{\partial a}{\partial \theta}\frac{\partial k}{\partial \eta} - k\frac{\partial}{\partial \eta}\left(\frac{\partial a}{\partial \theta}\right) +$$

$$+\frac{\partial a}{\partial \eta}\frac{k_\varphi^2\cot\theta}{k} - \frac{ak_\varphi^2}{k^2}\cot\theta\frac{\partial k}{\partial \eta} + \frac{2ak_\varphi}{k}\cot\theta\frac{\partial k_\varphi}{\partial \eta} -$$

$$-\frac{ak_\varphi^2}{k\sin^2\theta}\frac{\partial \theta}{\partial \eta} - \frac{\partial k_\theta}{\partial \eta}\frac{dr}{dt} - k_\theta\frac{d}{dt}\left(\frac{\partial r}{\partial \eta}\right), (4)$$

$$\frac{\partial r}{\partial \eta}\sin\theta\frac{dk_\varphi}{dt} + r\cos\theta\frac{\partial \theta}{\partial \eta}\frac{dk_\varphi}{dt} + r\sin\theta\frac{d}{dt}\left(\frac{\partial k_\varphi}{\partial \eta}\right) =$$

$$= -\frac{\partial V_r}{\partial \varphi}\frac{\partial k_r}{\partial \eta} - k_r\frac{\partial}{\partial \eta}\left(\frac{\partial V_r}{\partial \varphi}\right) - \frac{\partial a}{\partial \varphi}\frac{\partial k}{\partial \eta} - k\frac{\partial}{\partial \eta}\left(\frac{\partial a}{\partial \varphi}\right) - \cos\theta\frac{\partial \theta}{\partial \eta}k_\varphi\frac{dr}{dt} -$$

$$-\sin\theta\frac{\partial k_\varphi}{\partial \eta}\frac{dr}{dt} - \sin\theta k_\varphi\frac{d}{dt}\left(\frac{\partial r}{\partial \eta}\right) - \frac{\partial k_\varphi}{\partial \eta}r\cos\theta\frac{d\theta}{dt} - k_\varphi\frac{\partial r}{\partial \eta}\cos\theta\frac{d\theta}{dt} +$$

$$+k_\varphi r\sin\theta\frac{\partial \theta}{\partial \eta}\frac{d\theta}{dt} - k_\varphi r\cos\theta\frac{d}{dt}\left(\frac{\partial \theta}{\partial \eta}\right),$$

where:

$$\frac{\partial V_r}{\partial \eta} = \sum_\alpha \frac{\partial V_r}{\partial r_\alpha}\frac{\partial r_\alpha}{\partial \eta}, \quad \frac{\partial a}{\partial \eta} = \sum_\alpha\left(\frac{\partial a}{\partial r_\alpha}\frac{\partial r_\alpha}{\partial \eta} + \frac{\partial a}{\partial k_\alpha}\frac{\partial k_\alpha}{\partial \eta}\right), \quad \frac{\partial k}{\partial \eta} = \frac{1}{k}\sum_\alpha k_\alpha\frac{\partial k_\alpha}{\partial \eta},$$

$$\frac{\partial}{\partial \eta}\left(\frac{\partial a}{\partial k_\beta}\right) = \sum_\alpha\left(\frac{\partial}{\partial r_\alpha}\left(\frac{\partial a}{\partial k_\beta}\right)\frac{\partial r_\alpha}{\partial \eta} + \frac{\partial}{\partial k_\alpha}\left(\frac{\partial a}{\partial k_\beta}\right)\frac{\partial k_\alpha}{\partial \eta}\right),$$

$$\frac{\partial}{\partial \eta}\left(\frac{\partial a}{\partial r_\beta}\right) = \sum_\alpha\left(\frac{\partial}{\partial r_\alpha}\left(\frac{\partial a}{\partial r_\beta}\right)\frac{\partial r_\alpha}{\partial \eta} + \frac{\partial}{\partial k_\alpha}\left(\frac{\partial a}{\partial r_\beta}\right)\frac{\partial k_\alpha}{\partial \eta}\right),$$

$$\frac{\partial}{\partial \eta}\left(\frac{\partial V_r}{\partial r_\beta}\right) = \sum_\alpha \left(\frac{\partial}{\partial r_\alpha}\left(\frac{\partial V_r}{\partial r_\beta}\right)\frac{\partial r_\alpha}{\partial \eta}\right), \quad r_{\alpha,\beta} = \{r, \theta, \varphi\}, \quad k_{\alpha,\beta} = \{k_r, k_\theta, k_\varphi\}.$$

As the ray coordinates η_1 and η_2, we can choose, for instance, angles of the ray escape from a point source at the initial moment. Note that the ray coordinates need not be explicitly determined when the adjoint system is being derived. This becomes essential to specify initial values for desired functions.

Thus, to calculate propagation of a linear wave and its intensity, at first we have to integrate numerically ray equations system (1) and adjoint system (4) and then determine the amplitude variations by means of (3).

A nonlinear flat disturbance in an ideal homogeneous medium is described by a simple wave solution and propagates at the supersonic speed determined by its amplitude (Kulikovsky and Lyubimov, 2005). A fast-mode simple-wave element with a plasma velocity component u normal to the front moves at $a + \kappa u$, where $\kappa = (1/a)\left(d\left(\rho a\right)/d\rho\right)$ is the numerical coefficient depending both on the plasma beta and the angle between the wave vector and the magnetic field. We do not give here the bulky explicit expression for κ. Note only that values of κ are restricted by the limits: $(\gamma + 1)/2 \leq \kappa \leq 3/2$, with γ being the adiabatic index. The fact that each simple-wave element travels at its own speed causes the wave profile deformation and an appearance of a discontinuity. If a moderate amplitude simple wave has a triangular profile before the discontinuity appears, it will take a shape of the right-angled triangle after the discontinuity forms, with the discontinuity being a leading edge of the disturbance. Note that any nonlinear disturbance profile of a finite duration tends asymptotically to this shape. Let U_{sh} be a jump of the plasma velocity component u in the discontinuity. Then, in the nonlinear geometrical acoustics approximation, the discontinuity moves at a speed of $a + \kappa U_{sh}/2$. Taking into account this increase in a wave front speed in the ray equations, we are able to correctly describe propagation of weak shock waves. Then ray equation system (1) becomes (Uralova and Uralov, 1994):

$$
\begin{aligned}
\frac{dr}{dt} &= V_r + \left(a + \frac{\kappa U_{sh}}{2}\right)\frac{k_r}{k} + k\frac{\partial a}{\partial k_r}, \\
r\frac{d\theta}{dt} &= \left(a + \frac{\kappa U_{sh}}{2}\right)\frac{k_\theta}{k} + k\frac{\partial a}{\partial k_\theta}, \\
r\sin\theta\frac{d\varphi}{dt} &= \left(a + \frac{\kappa U_{sh}}{2}\right)\frac{k_\varphi}{k} + k\frac{\partial a}{\partial k_\varphi}, \\
\frac{dk_r}{dt} &= -\frac{\partial V_r}{\partial r}k_r - \frac{\partial a}{\partial r}k + \frac{a}{kr}\left(k_\theta^2 + k_\varphi^2\right), \\
r\frac{dk_\theta}{dt} &= -\frac{\partial V_r}{\partial \theta}k_r - \frac{\partial a}{\partial \theta}k + \frac{a}{k}k_\varphi^2\cot\theta - k_\theta\frac{dr}{dt}, \\
r\sin\theta\frac{dk_\varphi}{dt} &= -\frac{\partial V_r}{\partial \varphi}k_r - \frac{\partial a}{\partial \varphi}k - \sin\theta k_\varphi\frac{dr}{dt} - k_\varphi r\cos\theta\frac{d\theta}{dt}.
\end{aligned}
\tag{5}
$$

The generally accepted method of nonlinear geometrical acoustics ignores additional term $\kappa U_{sh}/2$ as small. However, it is the term that is responsible for wave deceleration due to the amplitude damping. Besides, estimations within the

framework of the perturbation theory suggest that the ray pattern variation due to nonlinearity is a correction of the same order of magnitude that the nonlinear variation of the wave amplitude is. It is therefore important to take this into account in the nonlinear geometrical acoustics approximation.

Ray equation system (5) is not closed now because it includes the wave amplitude. In the linear approximation, an amplitude variation can be determined from (3). The nonlinear wave amplitude undergoes the additional damping associated with energy dissipation in a discontinuity. As the amplitude, we take a value of jump U_{sh}. Variations of amplitude U_{sh} and duration T_{sh} of a weak shock wave having a triangular compression phase may be calculated as (Uralov, 1982):

$$U_{sh} = u_1 \left(1 + \frac{\tau_1}{T_*}\right)^{-1/2}, \quad T_{sh} = T_* \left(1 + \frac{\tau_1}{T_*}\right)^{1/2}, \quad \frac{d\tau_1}{dt} = \frac{\kappa u_1}{q_n} \qquad (6)$$

where τ_1 is the duration increment of the simple wave with an amplitude of u_1; T_* is the initial duration of the disturbance. Note that laws (6) of a weak shock wave damping are derived by using values of the amplitude and duration of a simple wave, from which the discontinuity forms. A value of u_1 can be determined from the expression similar to (3).

Thus, solving numerically of 19 ordinary differential equations (5), (4), and (6) enables us to compute propagation of a weak shock wave in an inhomogeneous medium, its amplitude and duration.

3. Analytical Modeling of Wave Propagation

In this section, we employ the nonlinear geometrical acoustics method to describe propagation of large-scale wave-like transients, namely EUV and Moreton waves. With respect to "EUV wave" phenomena, we address only those disturbances, which associated with a fast-mode MHD shock wave.

To calculate propagation of a shock wave, we have to specify the solar corona model as well as a position and parameters of the shock wave at the initial moment. We use a simple hydrostatic corona model to demonstrate main particularities of the method and compare results with those obtained in the linear approximation. The corona is considered to be isothermal with temperature $T = 1.5 \times 10^6$ K and sound speed $c = 181$ km s^{-1}. The number density of plasma is distributed in accordance with the barometric law (for details see, *e.g.*, Mann *et al.*, 1999):

$$n(r) = n_0 \exp\left(\frac{R_\odot}{H}\left(\frac{R_\odot}{r} - 1\right)\right), \qquad (7)$$

where $n_0 = n(R_\odot) = 3 \times 10^8$ cm^{-3} is the number density at the base of the corona, $R_\odot$ the solar radius, $H = 2R_{gas}T/\widetilde{m}M_H g_\odot \approx 70$ Mm the density scale height, $g_\odot$ the acceleration of gravity on the solar surface, M_H the molar mass of hydrogen, $\widetilde{m} = 1.27$ the average atomic weight of an ion, and R_{gas} the gas
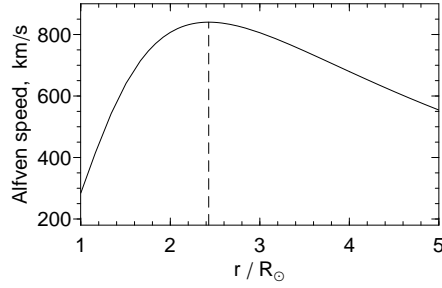
Figure 1. The Alfvén speed distribution in solar corona model (7), (8).

constant. Let us assume a magnetic field having only a radial component (for details see, *e.g.*, Mann *et al.*, 2003):

$$B_r = \pm B_0 \left(\frac{R_\odot}{r} \right)^2 , \qquad (8)$$

where $B_0 = 2.3$ G is its value at the base of the corona. The sign in (8) depends on the solar hemisphere, but it is no object in the case considered. The same model was applied by Uchida (1968).

In the corona model (7) and (8), the Alfvén speed increases with height, peaking at $R_\odot^2/4H = 2.43$ $R_\odot$ (Figure 1). Refraction makes ray trajectories curved to regions of the lower Alfvén speed. The solar corona has therefore waveguide properties. A portion of the wave energy flux is captured by the coronal waveguide and propagates along the solar surface, giving rise to an EUV and Moreton wave. In the treatment used, the EUV front is observable due to the plasma compression produced by the coronal shock wave. Since the plasma density decreases rapidly with a height, a plasma layer near the solar surface contributes substantially to the EUV front emission. The layer thickness is about density scale height H. So, to estimate the EUV front position, we have to find the intersection line of the calculated shock front and a spherical surface of radius $\lesssim (R_\odot + H)$. The Moreton wave corresponds to the chromospheric trail of the coronal shock wave, *i.e.* it can be found as the intersection line of the shock front and the upper chromosphere.

For modeling, it is important to assign the initial characteristics of a shock wave and its start position. We have to specify the initial duration (or length) of the wave and its initial amplitude on some surface. In this study, these values are given according to the strong point-like explosion theory. The wave source located at a height of 80 Mm is characterized by the energy $\tilde{\varepsilon}$ whose release produces a shock wave. When the wave covers a distance of $\Lambda = (\tilde{\varepsilon}/\rho_* a_*^2)^{1/3}$, with ρ_* and a_* being respectively the plasma density and the fast-mode speed at the explosion point, the compression phase profile of the wave is assumed to be triangular. The compression phase length is equal to Λ and the amplitude is χa_*, with χ being the coefficient of the order of unity. In this paper, we employ a value $\chi = 1$ except for the calculations given in Figure 7. The initial duration of the compression phase is supposed to equal to $T_* = \Lambda(\mathbf{k})/a_*(\mathbf{k})$. We
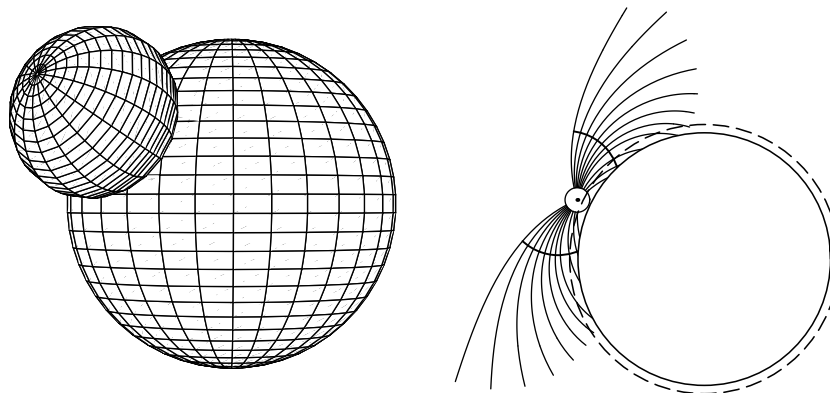
Figure 2. Propagation of a coronal shock wave as seen in a 3D image (left) and a 2D section with ray trajectories (right). The solid arcs drawn across the rays represent shock wave fronts. The dashed line marks a height of 60 Mm above the solar surface. The wave front velocity along this line corresponds to the velocity of an EUV wave. The wave source height is 80 Mm.

believe that a shock wave arises on the periphery of an active region located within the explosion cavity Λ. This manner to assign initial values does not rely on a specific mechanism of the wave initiation. It is essential only that the energy release producing a shock wave is impulsive. For instance, a wave can be produced by a compact piston acting for a short term (an abruptly accelerating filament and its magnetic envelope).

Figures 2–7 present the results of our modeling. Figure 2 illustrates a 3D image of the shock wave front and the respective 2D section including ray trajectories. The rays go out from the initial surface of size Λ. The wave front inclines over the solar surface, with its inclination increasing in time.

Figure 3 shows the distance-time plots of EUV waves (a) as well as the time plots of their velocities (b) along the surface 60 Mm (relative to the solar surface). The curves are given for different values of the wave source energy $\tilde{\varepsilon}$ or different values of the initial shock wave length, as it follows from $\Lambda = (\tilde{\varepsilon}/\rho_* a_*^2)^{1/3}$. The EUV wave velocity decreases appreciably due to the nonlinear damping of the coronal wave amplitude. After the amplitude has substantially decreased, the shock wave propagates as linear one. In Figure 3b, one can see this fact as approaching asymptotically the upper curves to the dotted one corresponding to a linear EUV wave and as aligning the curves in Figure 3a. Having reached its minimum, the wave velocity slightly increases. This is due to the shock front inclination over the solar surface that becomes more and more significant with time and associated with the waveguide properties of the lower quiet Sun's corona. The larger the wave front inclination, the higher the Moreton and EUV wave velocity. Note that calculated Moreton and EUV wave acceleration must be difficult to observe since it occurs when the wave amplitude becomes low (see Figure 5).

Figure 4 shows positions (a) counted along the surface and velocities (b) of a Moreton wave (thick lines) and an EUV wave (thin lines), which are produced by a single coronal wave. The dotted lines correspond to a linear coronal wave
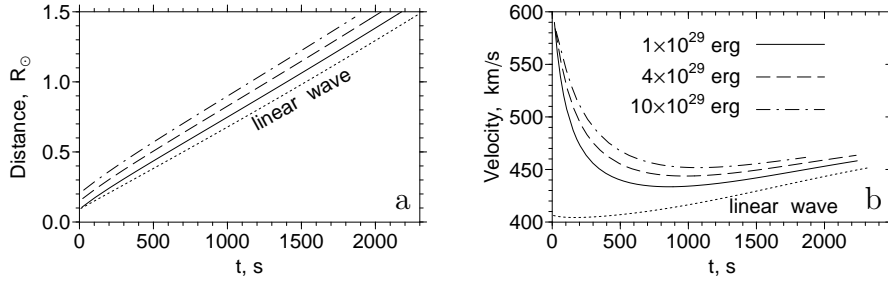
Figure 3. The distance-time plot of EUV waves (a) and the time plot of their velocities (b) along the surface 60 Mm for different energies $\tilde{\varepsilon}$ specified in panel b. The lowest (dotted) line represents a linear EUV wave.
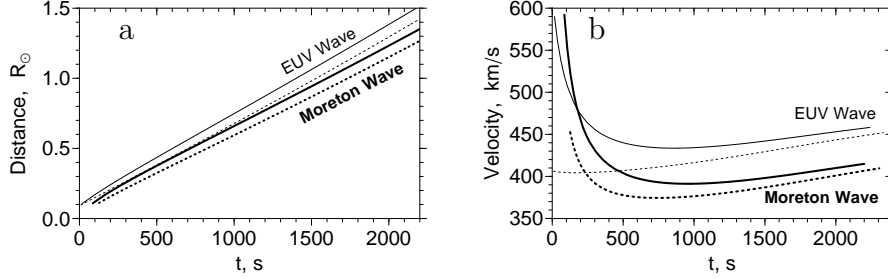

Figure 4. The kinematic plots of a Moreton wave (thick) and an EUV wave (thin), which are produced by a single coronal wave in the linear (dotted) and nonlinear (solid) consideration.

and the solid lines are for a shock one. The linear Moreton wave velocity is lower because the Alfvén speed at the corona base is smaller than that at a height of 60 Mm. Note that a Moreton wave decelerates even in the linear case. This fact is associated with the initial wave source position at a height of 80 Mm above the photosphere. The EUV wave in the linear case does not decelerate since the wave source is located roughly at the same height that the EUV wave is (a little bit higher the dashed line in Figure 2).

Increase in a propagation velocity of the shock wave front at a larger height results in a front inclination. So, one can observe the offset between shock wave signatures at different heights. Inclination increase with time determines evolution of the offset. Besides, its time evolution is also determined by the observer position and the sight angle. Such a consideration demonstrates a possibility to explain the offset between Moreton and EUV waves as well as the HeI-Hα offset observed by Vršnak *et al.* (2002b) since waves in the He I 10830 Å line are similar morphologically to EUV ones.

Figure 5 presents time dependence of the EUV wave amplitude for different values of the wave source energy $\tilde{\varepsilon}$. A disturbance having higher $\tilde{\varepsilon}$ and the greater length decays more slowly as it follows from (6) and seen in Figure 5. The Moreton wave amplitude varies in a similar manner, but it has smaller values.

Another effect associated with nonlinearity of an EUV wave is increase in its duration T_{sh} and, respectively, length $L = aT_{sh}$ (also referred to as the wave profile broadening). In the linear case, the wave duration is constant (under the
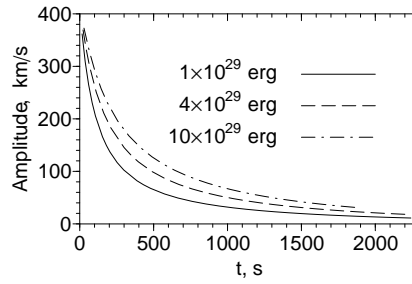
Figure 5. The time variation of the EUV wave amplitude for different energies $\tilde{\varepsilon}$ of the wave source.
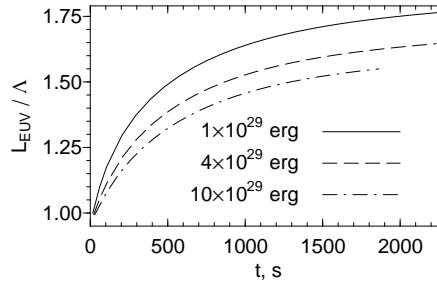

Figure 6. The time dependence of the EUV wave length relative to its initial size for different energies $\tilde{\varepsilon}$.

assumption of a steady-state medium). Figure 6 gives the time plot of the ratio of the EUV wave length to its initial size Λ. If initial amplitudes of disturbances are equal, a relative extension will be faster for disturbances having the lower initial energy (and the shorter initial length).

With respect to the damping of shock waves having the same initial lengths, amplitude decrease is faster for a wave with a higher amplitude. Therefore, shock waves with different initial amplitudes decay to the same level after approximately equal intervals (Figure 7, solid curves). For comparison, we also plot the amplitude curves of linear disturbances, which hold an initial ratio of the
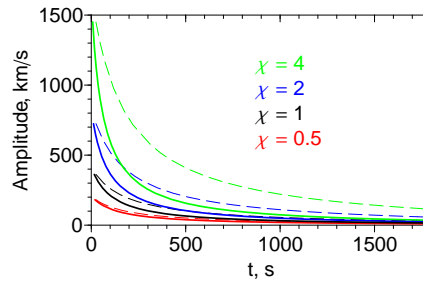

Figure 7. The amplitude damping of shock waves (solid lines) and linear ones (dashed lines), which is calculated for the wave source energy $\tilde{\varepsilon} = 10^{29}$ erg and different initial amplitudes. The initial amplitude values are specified in the figure as ratios χ of those to a fast-mode speed in the wave source.

wave amplitudes throughout propagation. The mentioned property of nonlinear waves (in Figure 7) allows us to be not precise about the value of the initial wave amplitude. Therefore, we can use the value that follows from the strong point-like explosion theory.

4. Discussion and Conclusion

We have modeled propagation of shock-associated EUV waves and Moreton waves, using the nonlinear geometrical acoustics method. This method takes into account characteristic properties of nonlinear waves: i) dependence of the wave velocity on its amplitude, ii) wave energy dissipation in the shock front, and iii) wave duration increase with time. The method allows one to calculate nonlinear evolution of a shock wave and its propagation pattern. However, the generally accepted variant of this approach includes nonlinearity effects only for describing the amplitude and duration of a wave, and does not it for the wave velocity value. So, using such a non-self-consistent approach results in the loss of an important effect concerning wave kinematics.

We have applied another approach, appending the additional term to the ray equations. This has allowed the finite wave amplitude to be taken into account. We have solved self-consistently the modified ray equations and the equations describing the wave amplitude and duration evolution along a ray tube. It is this approach that has been developed in this paper to analyze coronal shock wave propagation along the solar surface.

One of the results of our analysis is deceleration of EUV and Moreton waves at the initial stage of propagation. Since we use the spherically symmetric and isothermal model of the solar corona, deceleration is a direct consequence of their nonlinearity. Thus, EUV and Moreton waves having the sufficient amplitude (and therefore being observable) have to decelerate in the quiet Sun's regions where average plasma parameters are constant along the solar surface. Note that the large-scale waves under study are registered just in these regions. Calculated wave deceleration is supported by the EUV and Moreton wave observations analyzed by Warmuth *et al.* (2001, 2004a). Also we notice here that EUV waves not associated with a coronal MHD wave show only slight or no deceleration (see, *e.g.*, Wills-Davey and Attrill, 2009).

The simple corona model also let us find other features of wave kinematics, *e.g.*, i) the wave source height contributes to the initial portion of a velocity plot, and ii) the rate of wave deceleration and damping becomes lower as the wave source energy (or the wave length, respectively) grows. All this findings will be applied for modeling EUV wave propagation in the 17 January 2010 event in companion Paper III (Grechnev *et al.*, 2010a).

Modeling waves in the linear approximation does not reveal their deceleration. On the contrary, linear waves undergo only small acceleration caused by a slightly increasing inclination of the coronal wave front over the solar surface. This effect was first discovered by Uchida (1968). However, because of the error that he made in the expression for the barometric distribution of the coronal plasma density (the scale height was halved), the wave front inclination over the solar surface

was very large. As a result, linear waves underwent considerable acceleration in the Uchida's original model.

Another important result of our modeling is duration (and length) increase of Moreton and EUV waves. This effect is also confirmed by observations (*e.g.*, Warmuth *et al.*, 2001; Veronig *et al.*, 2010). In contrast, a linear disturbance keeps its duration unchanged in a steady-state medium. Note that in the linear approximation, the wave amplitude and duration also vary due to the viscosity, the thermal conductivity and the finite plasma conductivity, however, these effects are negligible against nonlinear factors.

To summarize, we believe that wave deceleration and its duration increase, both being the attributes of shock wave evolution, point out a crucial role of nonlinearity in the behavior of EUV and Moreton waves (at least, it concerns some of them).

In conclusion, we will briefly discuss the method limitations for solving the shock wave propagation problem. The main limitation is associated with laws (6) of a shock wave damping, which are derived by using the relations for simple flat MHD waves in a homogeneous medium. So, we have to meet two requirements. First, the shock wave length should be smaller than the radius of curvature of the wave front and the smallest medium variation scale. The fulfilment of these conditions also ensures validity of the linear ray approximation (1), which involves actually even less limitations. The smallest variation scale in our modeling is that of plasma density. So, we realize that our computation lies at the boundary of applicability of nonlinear geometrical acoustics since characteristic shock wave length Λ and density scale $\rho/\left|\nabla\rho\right|$ are of the same order of magnitude.

Second, a nonlinear factor U_{sh}/a should be small. Under this condition, damping laws (6) are derived and this very condition ensures a correct calculation of the terms involving U_{sh} in ray equations system (5). With respect to the limitations of laws (6), the point-like atmospheric explosion theory (Kestenboim, Roslyakov, and Chudov, 1974) suggests that these laws satisfactory describe spherical shock wave propagation up to $U_{sh}/a \leq 1$. When we choose the initial value $U_{sh} = a$ in Section 3, we do not therefore go beyond the scope of the application of relations (6). However, ray equations (5) and equations (4) at $U_{sh}/a \approx 1$ are able to yield an error in calculations. Nevertheless, this error is insignificant due to the nearly spherical shape of the wave front at the initial phase of propagation and then it disappears owing to rapid decrease in U_{sh}.

References

Balasubramaniam, K. S., Pevtsov, A. A., and Neidig, D. F.: 2007, *Astrophys. J.* **658**, 1372.
Barnes, A.: 1992, *J. Geophys. Res.* **97**, 12105.

Blokhintsev, D. I.: 1981, *Acoustics of an Inhomogeneous Moving Medium*, 2nd edn., Nauka, Moscow (in Russian).

Gilbert, H. R., Holzer, T. E., Thompson, B. J., and Burkepile, J. T.: 2004, *Astrophys. J.* **607**, 540.

Grechnev, V. V., Uralov, A. M., Slemzin, V. A., Chertok, I. M., Kuzmenko, I. V., and Shibasaki, K.: 2008, *Solar Phys.* **253**, 263.

Grechnev, V. V., Afanasyev, An. N., Uralov, A. M., Chertok, I. M., Eselevich, M. V., Eselevich, V. G., Rudenko, G. V., and Kubo, Y.: 2010a, *Solar Phys.* Submitted.

Grechnev, V. V., Uralov, A. M., Chertok, I. M., Kuzmenko, I. V., Afanasyev, An. N., Meshalkina, N. S., Kalashnikov, S. S., and Kubo, Y.: 2010b, *Solar Phys.* Submitted.

Hudson, H.S., Khan, J.I., Lemen, J.R., Nitta, N.V., and Uchida, Y.: 2003, *Solar Phys.* **212**, 121.

Kestenboim, Kh. S., Roslyakov, G. S., and Chudov, L. A.: 1974, *The Point Explosion*, Nauka, Moscow (in Russian).

Khan, J. I., and Aurass, H.: 2002, *Astron. Astrophys.* **383**, 1018.

Kravtsov, Y. A., and Orlov, Y. I.: 1990, *Geometrical Optics of Inhomogeneous Media*, Springer-Verlag, Berlin.

Kulikovsky, A. G., and Lyubimov, G. A.: 2005, *Magnetic Hydrodynamics*, 2nd edn., Logos, Moscow (in Russian).

Landau, L. D., and Lifshitz, E. M.: 1987, *Fluid Mechanics*, 2nd edn., Pergamon Press, Oxford.

Mann, G., Klassen, A., Aurass, H., and Classen, H.-T.: 2003, *Astron. Astrophys.* **400**, 329.

Mann, G., Jansen, F., MacDowall, R.J., Kaiser, M.L., and Stone, R.G.: 1999, *Astron. Astrophys.* **348**, 614.

Moreton, G. E., and Ramsey, H. E.: 1960, *Pub. Astron. Soc. Japan* **72**, 357.

Muhr, N., Vršnak, B., Temmer, M., Veronig, A.M., and Magdalenić, J.: 2010, *Astrophys. J.* **708**, 1639.

Narukage, N., Eto, S., Kadota, M., Kitai, R., Kurokawa, H., and Shibata, K.: 2004, in A.V. Stepanov, E.E. Benevolenskaya, and A.G. Kosovichev (eds.), Multi-Wavelength Investigations of Solar Activity, Proc. IAU Symp. **223**, 367.

Narukage, N., Hudson, H.S., Morimoto, T., Akiyama, S., Kitai, R., Kurokawa, H., and Shibata, K.: 2002, *Astrophys. J.* **572**, L109.

Patsourakos, S., Vourlidas, A., Wang, Y. M., Stenborg, G., and Thernisien, A.: 2009, *Solar Phys.* **259**, 49.

Temmer, M., Vršnak, B., Žic, T., and Veronig, A. M.: 2009, *Astrophys. J.* **702**, 1343.

Uchida, Y.: 1960, *Pub. Astron. Soc. Japan* **12**, 376.

Uchida, Y.: 1968, *Solar Phys.* **4**, 30.

Uchida, Y.: 1974, *Solar Phys.* **39**, 431.

Uchida, Y., Altschuler, M. D., and Newkirk, G., Jr.: 1973, *Solar Phys.* **28**, 495.

Uralov, A. M.: 1982, *Magnitnaya Gidrodinamika* No. 1, 45 (in Russian).

Uralova, S. V., and Uralov, A. M.: 1994, *Solar Phys.* **152**, 457.

Veronig, A. M., Muhr, N., Kienreich, I. W., Temmer, M., and Vršnak, B.: 2010, *Astrophys. J.* **716**, L57.

Vršnak, B., and Lulić, S.: 2000, *Solar Phys.* **196**, 157.

Vršnak, B., Magdalenić, J., Aurass, H., and Mann, G.: 2002a, *Astron. Astrophys.* **396**, 673.

Vršnak, B., Warmuth, A., Brajša, R., and Hanslmeier, A.: 2002b, *Astron. Astrophys.* **394**, 299.

Vršnak, B., Magdalenić, J., Temmer, M., Veronig, A., Warmuth, A., Mann, G., Aurass, H., and Otruba, W.: 2005, *Astrophys. J.* **625**, L67.

Wang, Y.-M.: 2000, *Astrophys. J.* **543**, L89.

Warmuth, A., Mann, G., and Aurass, H.: 2005, *Astrophys. J.* **626**, L121.

Warmuth, A., Vršnak, B., Aurass, H., and Hanslmeier, A.: 2001, *Astrophys. J.* **560**, L105.

Warmuth, A., Vršnak, B., Magdalenić, J., Hanslmeier, A., and Otruba, W.: 2004a, *Astron. Astrophys.* **418**, 1101.

Warmuth, A., Vršnak, B., Magdalenić, J., Hanslmeier, A., and Otruba, W.: 2004b, *Astron. Astrophys.* **418**, 1117.

White, S. M., and Thompson, B. J.: 2005, *Astrophys. J.* **620**, L63.

Wills-Davey, M. J., and Attrill, G. D. R.: 2009, *Space Sci. Rev.* **149**, 325.

Žic, T., Vršnak, B., Temmer, M., and Jacobs, C.: 2008, *Solar Phys.* **253**, 237.